Investigating Vector-Borne and Zoonotic Diseases with Remote Sensing and GIS

29

Stephen C. Guptill and Chester G. Moore

Contents

29.1 Introduction

For centuries, people have been intuitively aware of the relationships between human health and the environment. Today, geographic information systems (GIS), remote sensing satellites, and other technologies are providing scientists with the tools and the data to make clear the geographic relationships between the habitats of disease agents, their vectors and vertebrate hosts, and the occurrence of disease in the human population. Although the utility of the foregoing tools as an aid to epidemiology was pointed out 30 years ago (Cline 1970), the medical community has been slow to put them to use.

In this discussion, we provide an introduction to remote sensing technology and then use vector-borne and zoonotic diseases to demonstrate some current and potential uses of remote sensing, GIS, and related technologies for the surveillance, prevention, and control of disease. Vector-borne is defined as those diseases that are transmitted from one vertebrate host to another by an invertebrate, usually an insect, a tick, or a snail. A zoonosis (pl. zoonoses) is a disease that normally exists in a non-human host, or reservoir. For example, passerine birds are the natural hosts of several viruses that can infect humans. Many vector-borne diseases are also zoonoses (for example, yellow fever, Lyme disease, and plague).

There are several reasons for choosing this group of diseases as our examples. First, these diseases account for a large portion of the annual global morbidity and mortality. It is estimated that 41% of the world's population (about 2.3 billion people) live in areas with malaria risk (Gratz 1999). Of approximately 300–500 million people who become infected each year, some 1.5–2.7 million die from this disease. Dengue, a virus related to yellow fever, attacks as many as 50–100 million people each year, and there are more than 250,000 cases of the more severe forms of dengue hemorrhagic fever and dengue shock syndrome. Rabies, a zoonosis, is responsible for at least 35,000–45,000 deaths

S.C. Guptill (✉)
United States Department of the Interior, United States Geological Survey, Reston, VA, USA
e-mail: sguptill@guptillgeoscience.com

C.G. Moore
Department of Microbiology, Immunology and Pathology, School of Veterinary Medicine and Biomedical Sciences, Colorado State University, Fort Collins, CO, USA

O. Selinus et al. (eds.), *Essentials of Medical Geology: Revised Edition*,
DOI 10.1007/978-94-007-4375-5_29,

each year. Second, these diseases—especially the zoonoses—are naturally occurring systems that are impacted by a wide variety of physical and biotic factors that may be susceptible to remote measurement (e.g., Ostfeld et al. 1996). Finally, there is considerable concern about the potential impact of global change on the dynamics and spread of these diseases (e.g., Shope 1992; Reeves et al. 1994; Martens et al. 1995; Jetten and Focks 1997).

29.2 Fundamentals of Remote Sensing

Remote sensing is a technology that involves the analysis and interpretation of images gathered through techniques that do not require direct contact with the object. Electromagnetic radiation sensors are used to record images of the environment. The sensors used in these devices can detect radiation from the ultraviolet through the visible and infrared spectra to microwave radar. In studying the Earth, the remote sensing devices are usually deployed in aircraft or Earth-orbiting satellites. For convenience, in the remainder of this paper, we will generally refer to remote sensing satellites, but the concepts and principles also apply to remote sensing instruments carried aboard aircraft.

Remote sensing satellites are designed to collect various types of information about the Earth's surface and atmosphere. The combination of spatial resolution of the sensor, the wavelengths detected by that sensor, and the frequency of data collection determine the types of applications for which the satellite will collect useful information. These design parameters must be weighed one against another, as they are somewhat mutually exclusive. Each of these parameters will be examined below along with descriptions of how they have been implemented in various operational systems.

29.2.1 Electromagnetic Spectrum

Electromagnetic radiation (EMR) extends over a wide range of energies and wavelengths (frequencies). A narrow range of EMR extending from 0.4 to 0.7 μm, the interval detected by the human eye, is known as the *visible region* (also referred to as *light*, but physicists often use that term to include radiation beyond the visible). White light contains a mix of all wavelengths in the visible region. The distribution of the continuum of all radiant energies can be plotted either as a function of wavelength or of frequency in a chart known as the electromagnetic spectrum.

Using spectroscopes and other radiation detection instruments, scientists have arbitrarily divided the electromagnetic spectrum into regions or intervals and applied descriptive names to them. At the very energetic (high frequency and short wavelength) end are gamma rays and x-rays, whose wavelengths are normally measured in angstroms (Å), which in the metric scale are in units of 10^{-8} cm. Radiation in the ultraviolet extends from about 300–4,000 Å. It is convenient to measure the mid-regions of the spectrum in one of two units: micrometers (μm), which are multiples of 10^{-6} m or nanometers (nm), based on 10^{-9} m. The visible region occupies the range between 0.4 and 0.7 μm, or its equivalents of 4,000–7,000 Å or 400–700 nm. The infrared region (IR), spanning between 0.7 and 100 μm, has four subintervals of special interest: (1) reflected IR (0.7–3.0 μm); (2) its film responsive subset, the photographic IR (0.7–0.9 μm); and (3) thermal bands at 3–5 μm and (4) 8–14 μm. Longer wavelength intervals are measured in units ranging from millimeters to centimeters to meters. The microwave region spreads across 0.1–100 cm, which includes the entire interval used by radar systems. These systems generate their own active radiation and direct it toward targets of interest. The lowest frequency–longest wavelength region beyond 100 cm is the radio bands, from VHF (very high frequency) to ELF (extremely low frequency). Within any region, a collection of continuous wavelengths can be partitioned into discrete intervals called *bands*.

Most remote sensing is conducted above the Earth either within or above the atmosphere. The gases in the atmosphere interact with solar irradiation and with radiation from the Earth's surface. The atmosphere itself is excited by EMR and thus becomes another source of released photons. Figure 29.1 (Short 2003) is a generalized diagram which shows relative atmospheric radiation transmission of different wavelengths.

Shaded zones mark minimal passage of incoming and/or outgoing radiation, whereas white areas denote atmospheric windows in which the radiation does not interact much with air molecules and hence, is not absorbed.

Most remote sensing instruments on air or space platforms operate in one or more of these windows by making their measurements with detectors tuned to specific frequencies (wavelengths) that pass through the atmosphere. However, some sensors, especially those on meteorological satellites, directly measure absorption phenomena, such as those associated with carbon dioxide (CO_2) and other gaseous molecules. Note that the atmosphere is nearly opaque to electromagnetic radiation in part of the mid-IR and all of the far-IR regions. In the microwave region, by contrast, most of this radiation moves through unimpeded, so radar waves reach the surface.

Remote sensing of the Earth traditionally has used reflected energy in the visible and infrared and emitted energy in the thermal infrared and microwave regions to gather radiation that can be analyzed numerically or used to generate images whose variations represent different intensities of photons associated with a range of wavelengths that are received at the sensor. This gathering of a (continuous or discontinuous) range(s) of wavelengths is the essence of what is usually termed multispectral remote sensing (Short 2003).

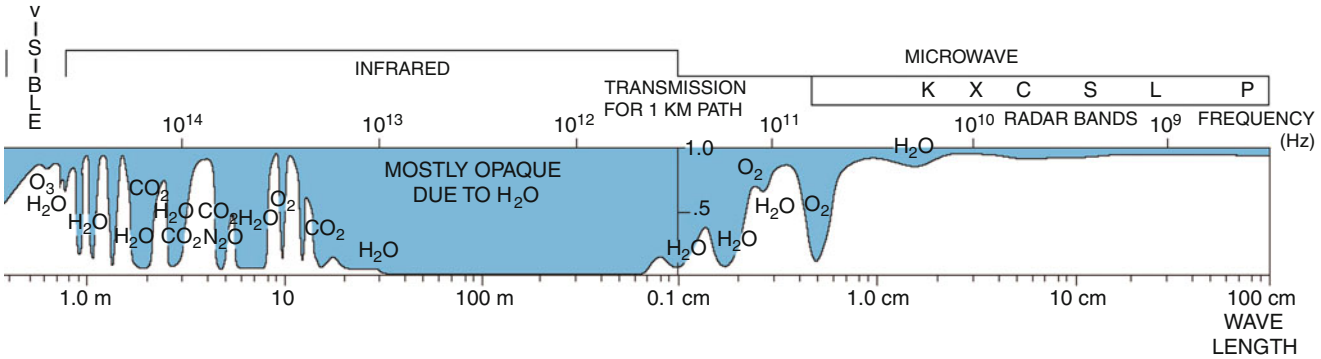

Fig. 29.1 Electromagnetic spectrum showing areas of transmission (*in white*) and areas of atmospheric absorption (*in blue*)

29.2.2 Spatial, Temporal, and Spectral Resolution

Spatial, temporal, and spectral resolution are three parameters that largely determine the characteristics of the data collected by a remote sensing instrument and thus to some degree the applications for which those data can be used.

The orbital characteristics of the satellite are the primary determinant of its temporal characteristics, that is, the time required for the sensor to re-image the same geographic location on the Earth. This can range from a daily revisit for the advanced very high resolution radiometer (AVHRR) sensor on the National Oceanic and Atmospheric Administration (NOAA) satellite to a 16-day revisit time for Landsat 7. Most satellites image the area directly below the sensor (nadir). However, some satellites are designed to point the sensor off-nadir, allowing the satellite to image the target area more frequently.

The imaging sensors are designed to collect energy from a certain portion or portions of the electromagnetic spectrum. For example a "panchromatic" sensor collects one set of data (i.e., a grayscale image) across a broad spectrum of visible and near infrared energy (450–900 nm). In contrast a hyperspectral sensor, like Hyperion, collects 250 bands of data, each 10 nm in width from 43–2,400 nm. Figure 29.2a–d shows the ways in which different features are highlighted or hidden depending on the band combinations used to make the image.

Spatial resolution refers to the smallest unit of area within which the sensor integrates EMR. More commonly it is referred to as "pixel size." This size is basically determined by the height of the orbit above the Earth and the magnification power of the optics on the sensor. As of the fall of 2003 the QuickBird satellite obtains the highest spatial resolution image with a 61-cm (approximately 2 ft) pixel size panchromatic (black and white) image collected in the 450- to 900-nm band. The detail available at this resolution can be seen in Fig. 29.3 which is an image of the Eiffel Tower taken on April 9, 2002. The coarsest image commonly used in our applications is from the AVHRR sensor, with a ground resolution of approximately 1 km.

Using digital image processing, satellite data of varying resolutions can be combined. In the example below, QuickBird 61-cm panchromatic imagery is combined with 2.4-m multispectral imagery (collected at the same time) to create a color image with 61-cm resolution. This image of Prague (Fig. 29.4) was taken on August 17, 2002, and shows the extent of flood damage to the city.

29.3 Remote Sensing Satellites

Remote sensing instruments fall naturally into three groups based on their principal applications: land observation, meteorology, or oceanography. However, many of the satellites provide useful information for more than one set of applications. Here, compiled by Nicholas Short (2003), are the principal remote sensing spacecraft flown by the United States and other nations (identified in parentheses) along with the launch date (if more than one in a series, this date refers to the first one put successfully into orbit):

1. *Land observation:* Government satellites—Landsat 1–7 (1973); Seasat (1978); HCMM (1978); RESURS (Russia) (1985); *IRS* 1A–1D (India) (1986); ERS 1–2 (1991); JERS 1–2 (Japan) (1992); Radarsat (Canada) (1995); ADEOS (Japan) (1996); Terra (1999)
   Commercial satellites—SPOT (France) (1986); Resurs-01 series (Russia) (1989; became commercial in the 1990s); Orbview-2 (U.S.) (1997); SPIN-2 (Russia) (1998); IKONOS (U.S.) (1999); QuickBird (U.S.) (2001); EROS A (ImageSat International; Israel) (2002)
2. *Meteorological observation*: TIROS 1–9 (1960); Nimbus 1–7 (1964); ESSA 1–9 (1966); ATS (g = geostationary) 1–3 (1966); DMSP series I (1966); the Russian Kosmos (1968) and Meteor series (1969); ITOS series (1970); SMS(g) (1975); GOES(g) series (1975); NOAA 1–5 (1976); DMSP series 2 (1976); GMS (Himawari) (g)

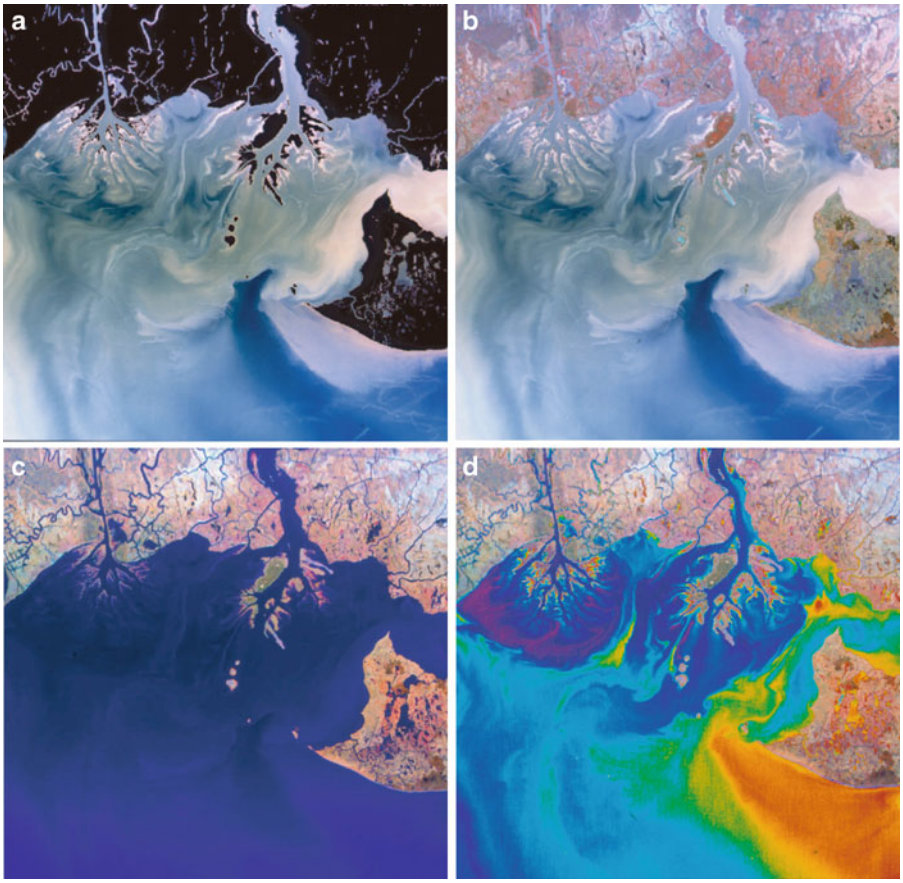

Fig. 29.2 Atchafalya Bay, Louisiana (Courtesy NASA). (**a**) *Bands* showing natural color, (**b**) *bands* showing color-infrared, (**c**) *bands* showing middle-infrared, and (**d**) *bands* showing thermal radiation

Fig. 29.3 Panchromatic image of the Eiffel Tower, Paris, France, with resolution of 61 cm (Courtesy DigitalGlobe)

Fig. 29.4 Panchromatic/multispectral merged image of Prague Czechoslovakia with effective resolution of 61 cm (Courtesy DigitalGlobe)

series (Japan) (1977); Meteosat(g) series (Europe) (1978); TIROS-N series (1978); Bhaskara(g) (India) (1979); NOAA (6–14) (1982); Insat (1983); ERBS (1984); MOS (Japan) (1987); UARS (1991); TRMM (U. S./Japan) (1997); Envisat (European Space Agency) (2002); Aqua (2002)

3. *Oceanographic observations*: Seasat (1978); Nimbus 7 (1978) included the *CZCS*, the Coastal Zone Color Scanner that measures chlorophyll concentration in seawater; Topex-Poseidon (1992); SeaWiFS (1997)

The Committee on Earth Observation Satellites (CEOS), supported by NASA, maintains a comprehensive database that shows the basic characteristics of current and future planned remote sensing satellite systems. A dynamic version of this table can be found at http://database.eohandbook.com/database/missiontable.aspx. As of January 2012, there were over 100 operational earth observation satellites.

So what applications are addressed by the data collected from these instruments? As part of NASA's Earth Observing System program, Michael King (2000) has created a table that shows a variety of physical measurements and characterizations that can be constructed from remote sensing data. The measurements/characteristics are shown on the left. The satellite/sensor that collects the raw information used in this process is on the right.

Atmosphere	
Cloud properties (amount, optical properties, height)	MODIS, GLAS, AMSR-E, MISR, AIRS, ASTER, SAGE III
Radiative energy fluxes (top of atmosphere, surface)	CERES, ACRIM III, MODIS, AMSR-E, GLAS, MISR, AIRS, ASTER, SAGE III
Precipitation	AMSR-E
Tropospheric chemistry (ozone, precursor gases)	TES, MOPITT, SAGE III, MLS, HIRDLS, LIS
Stratospheric chemistry (ozone, ClO, BrO, OH, trace gases)	MLS, HIRDLS, SAGE III, OMI, *TES*
Aerosol properties (stratospheric, tropospheric)	SAGE III, HIRDLS, MODIS, MISR, OMI, GLAS
Atmospheric temperature	AIRS/AMSU-A, MLS, HIRDLS, TES, MODIS
Atmospheric humidity	AIRS/AMSU-A/HSB, MLS, SAGE III, HIRDLS, Poseidon 2/JMR/DORIS, MODIS, TES
Lightning (events, area, flash structure)	LIS
Solar radiation	
Total solar irradiance	ACRIM III, TIM
Solar spectral irradiance	SIM, SOLSTICE
Land	
Land cover and land use change	ETM+, MODIS, ASTER, MISR
Vegetation dynamics	MODIS, MISR, ETM+, ASTER
Surface temperature	ASTER, MODIS, AIRS, AMSR-E, ETM+

(*continued*)

(continued)

Atmosphere	
Fire occurrence (extent, thermal anomalies)	MODIS, ASTER, ETM+
Volcanic effects (frequency of occurrence, thermal anomalies, impact)	MODIS, ASTER, ETM+, MISR
Surface wetness	AMSR-E
Ocean	
Surface temperature	MODIS, AIRS, AMSR-E
Phytoplankton and dissolved organic matter	MODIS
Surface wind fields	SeaWinds, AMSR-E, Poseidon 2/JMR/DORIS
Ocean surface topography (height, waves, sea level)	Poseidon 2/JMR/DORIS
Cryosphere	
Land ice (ice sheet topography, ice sheet volume change, glacier change)	GLAS, ASTER, ETM+
Sea ice (extent, concentration, motion, temperature)	AMSR-E, Poseidon 2/JMR/DORIS, MODIS, ETM+, ASTER
Snow cover (extent, water equivalent)	MODIS, AMSR-E, ASTER, ETM +

In the sections below, a few of the most widely available and useful systems for analyzing environmental influences on human health will be characterized.

29.3.1 Landsat

The Landsat program has been in operation since the early 1970s. Since then, many different satellites have been sent into orbit. Beginning with Landsat 1 in 1972 and most recently Landsat 7, these satellites have taken thousands of images of the Earth and documented the rapidly changing landscape of the planet.

Landsat 7 was launched on April 15, 1999, from the Western Test Range aboard a Delta II expendable launch vehicle. At launch, the satellite weighed approximately 4,800 lb (2,200 kg). The spacecraft is about 14 ft long (4.3 m) and 9 ft (2.8 m) in diameter. It consists of a spacecraft bus that is provided under a NASA contract with Lockheed Martin Missiles and Space in Valley Forge, Pennsylvania, and the Enhanced Thematic Mapper Plus (ETM+) instrument, pro-cured under a NASA contract with Raytheon (formerly Hughes) Santa Barbara Remote Sensing in California.

The ETM + instrument is an eight-band multispectral scanning radiometer capable of providing high-resolution imaging information of the Earth's surface. It detects spectrally filtered radiation at visible, near-infrared, short-wave, and thermal infrared frequency bands from the sun-lit Earth in a 115-mile (183 km) wide swath when orbiting at an altitude of 438 miles (705 km). Nominal ground sample distances or pixel sizes are 49 ft (15 m) in the panchromatic band; 98 ft (30 m) in the six visible, near- and short-wave infrared bands; and 197 ft (60 m) in the thermal infrared band. A Landsat WorldWide-Reference System has catalogued the world's landmass into 57,784 scenes, each 115 miles (183 km) wide by 106 miles (170 km) long. The ETM + produces approximately 3.8 Gb of data for each scene. The seven bands have the following characteristics:

Band no	Wavelength interval (μm)	Spectral response	Resolution (m)
1	0.45–0.52	Blue-green	30
2	0.52–0.60	Green	30
3	0.63–0.69	Red	30
4	0.76–0.90	Near-IR	30
5	1.55–1.75	Mid-IR	30
6	10.40–12.50	Thermal-IR	120
7	2.08–2.35	Mid-IR	30

The satellite orbits the Earth at an altitude of approximately 438 miles (705 km) with a sun-synchronous, 98-degree inclination and a descending equatorial crossing time of 10 a.m. The orbit will be adjusted upon reaching orbit so that its 16-day repeat cycle coincides with the Landsat Worldwide Reference System. This orbit will be maintained with periodic adjustments for the life of the mission. A three-axis attitude control subsystem will stabilize the satellite and keep the instrument pointed toward Earth to within 0.05degrees. A state-of-the-art solid-state recorder capable of storing 380 Giga bits of data (100 scenes) is used to store selected scenes from around the world for playback over a U.S. ground station. In addition to stored data, real-time data from ETM + can be transmitted to cooperating international ground stations and to the U.S. ground stations.

These spectral bands allow ETM + to detect subtle variations in surface characteristics. For example, on the border between Chile and the Catamarca province of Argentina lies a vast field of currently dormant volcanoes. Over time, these volcanoes have laid down a crust of magma roughly 2 miles (3.5 km) thick. It is tinged with a patina of various colors that can indicate both the age and mineral content of the original lava flows. This is shown in Fig. 29.5.

The U.S. Geological Survey operates the Landsat 7 satellite. For more information on Landsat 7 including how to order data, go to http://landsat7.usgs.gov/index.php.

29.3.2 AVHRR

AVHRR is a broad-band, four- or five-channel (depending on the model) scanner, sensing in the visible, near-infrared, and thermal infrared portions of the electromagnetic spectrum. This sensor is carried on NOAA's Polar Orbiting

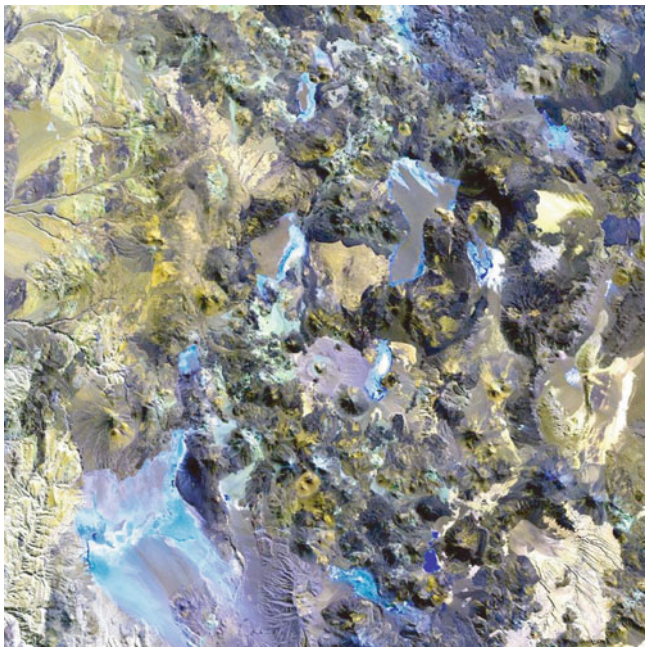

Fig. 29.5 Landsat ETM + image of Chile and Argentina (Courtesy USGS)

Environmental satellites (POES), beginning with TIROS-N in 1978 and most recently on the NOAA-15 (launched in 1998) and NOAA-16 (launched in 2000) satellites.

The AVHRR sensor provides for global (pole to pole) on-board collection of data from all spectral channels. Each pass of the satellite provides a 1,491-mile (2,399-km) wide swath. The satellite orbits the Earth 14 times each day from 517 miles (833 km) above its surface.

The average instantaneous field-of-view (IFOV) of 1.4 milliradians (mrad) yields a LAC/HRPT ground resolution of approximately 1.1 km at the satellite nadir from the nominal orbit altitude of 517 miles (833 km). The GAC data are derived from an on-board sample averaging of the full resolution AVHRR data. Four out of every five samples along the scan line are used to compute one average value and the data from only every third scan line are processed, yielding a 1.1 × 4 km resolution at nadir.

The current sensors cover five spectral bands as shown below:

Band	Wavelength (μm)	*IFOV* (mrad)
1	0.58–0.68	1.39
2	0.725–1.10	1.41
3	3.55–3.93	1.51
4	10.3–11.3	1.41
5	11.5–12.5	1.30

AVHRR data provide opportunities for studying and monitoring vegetation conditions in ecosystems including forests, tundra, and grasslands. Applications include agricultural assessment, land cover mapping, producing image maps of large areas such as countries or continents, and tracking regional and continental snow cover. AVHRR data are also used to retrieve various geophysical parameters such as sea surface temperatures and energy budget data.

Online requests for these data can be placed via the U.S. Geological Survey Global Land Information System (GLIS) interactive query system. The GLIS system contains metadata and online samples of Earth science data. With GLIS, you may review metadata, determine product availability, and place online requests for products. Additional data sets include the Alaska twice-monthly AVHRR and the U.S. Conterminous bi-weekly composites. These comprehensive time series data sets are calibrated, georegistered daily observations and twice-monthly maximum NDVI composites for each annual growing season. Global experimental bi-weekly normalized difference data, computed from Global Vegetation Index (GVI) data, are analyzed to monitor global vegetation and are a potential tool in global climatic studies.

Figure 29.6 shows an AVHRR image of the Mississippi River basin soon after the summer floods of 1993. This figure shows the extent of flooding and demonstrates the value of daily observations.

29.3.3 EOS Terra Spacecraft

On December 18, 1999, NASA launched the Earth Observing System (EOS) "flagship"—EOS Terra—to begin collecting a new 18-year global data set on which to base future scientific investigations about our complex home planet.

Physically, the EOS Terra spacecraft is roughly the size of a small school bus. It carries a payload of five state-of-the-art sensors that will study the interactions among the Earth's atmosphere, lands, oceans, and radiant energy (heat and light). Each sensor has unique design features that will enable EOS scientists to meet a wide range of science objectives.

EOS Terra orbits the Earth from pole to pole descending across the equator in the morning when cloud cover is minimal and its view of the surface is least obstructed. The satellite's orbit will be perpendicular to the direction of Earth's spin, so that the viewing swaths from each overpass can be compiled into whole global images. Over time, these global images will enable scientists to show and tell the stories of the causes and effects of global climate change.

The sensors on EOS Terra will not actively scan the surface (such as with laser beams or microwave pulses). Rather, the sensors work much like a camera. Sunlight that is reflected by Earth, and heat that is emitted from Earth, will pass through the apertures of Terra sensors. This radiant energy will then be focused onto specially designed detectors that are sensitive to selected regions of the electromagnetic spectrum that range from visible light to heat. The

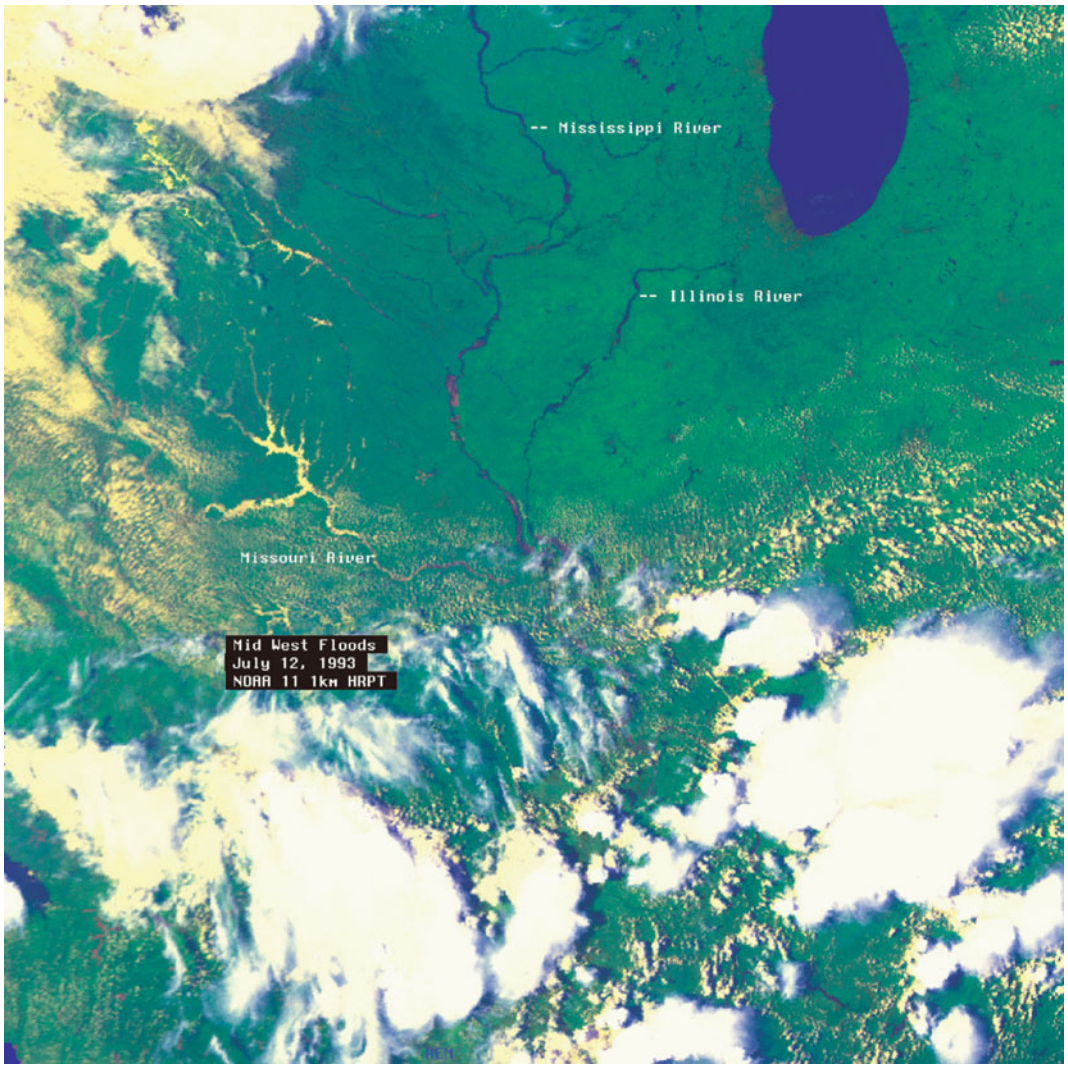

Fig. 29.6 AVHRR image of the central United States showing the Mississippi floods of 1993 (Courtesy NOAA)

information produced by these detectors will then be transmitted back to Earth and processed by computers into images that we can interpret.

The five Terra onboard sensors are

1. ASTER, or Advanced Spaceborne Thermal Emission and Reflection Radiometer
2. CERES, or clouds and earth's radiant energy system
3. MISR, or multi-angle imaging spectroradiometer
4. MODIS, or moderate-resolution imaging spectroradiometer
5. MOPITT, or measurements of pollution in the troposphere

MODIS provides continuous global coverage every 1–2 days and collects data from 36 spectral bands. Two bands (1–2) have a resolution of 250 m. Five bands (3–7) have a resolution of 500 m. The remaining bands (8–36) have a resolution of 1,000 m. The swath width for MODIS is 2,330 km. In its application, MODIS can be viewed in some ways as a higher resolution version of AVHRR. The MODIS image mosaic shown in Fig. 29.7a–c is a "greenness" map of the United States in January, April, and June 2001. The NDVI index (or greenness) is calculated from several of the MODIS bands and the seasonal variation in vegetation vigor can be seen in this image sequence.

ASTER provides 14 spectral bands with 15- to 90-m resolution, depending on bands. ASTER does not acquire data continuously, and its sensors are activated only to collect specific scenes upon request. The instrument consists of three separate telescopes, each of which provides different spectral range and resolution. The VNIR (visible and near-infrared) sensor provides 4 bands at 15-m resolution. The SWIR (short-wave infrared) sensor provides 6 bands at 30-m resolution. The TIR (thermal infrared) sensor provides 5 bands at 90-m resolution. The swath width for all sensors is 60 km.

ASTER data is generally available in the universal transverse mercator (UTM) projection, although some individual

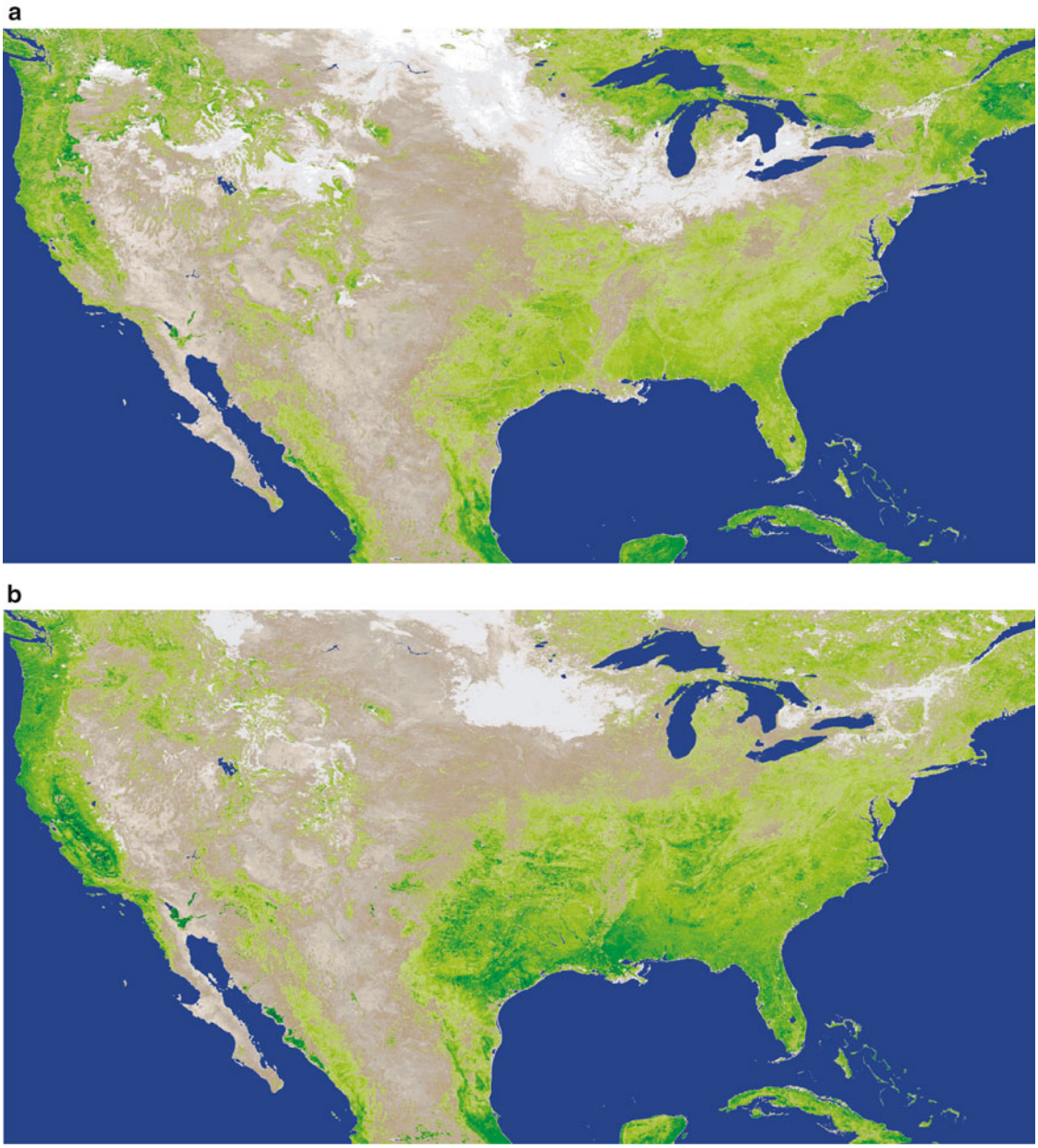

Fig. 29.7 MODIS NDVI image of the United States (Courtesy NASA). (**a**) January 2001, (**b**) April 2001, and (**c**) June 2001

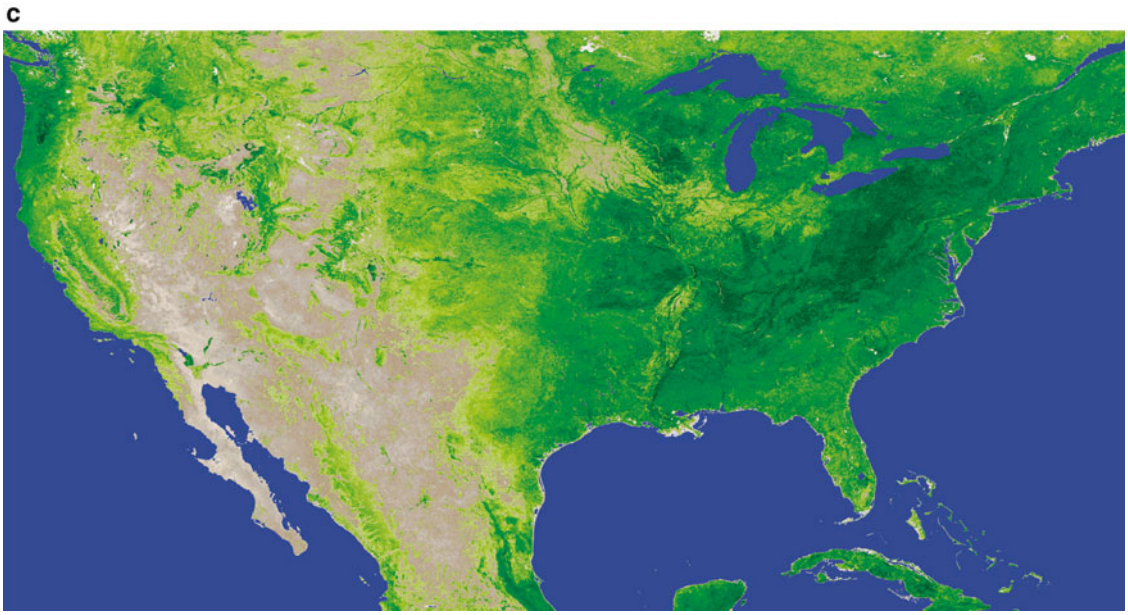

Fig. 29.7 (continued)

scenes may be cast to an alternative projection. The data is referenced to the World Geodetic Survey (WGS) System of 1984 (WGS84). Files are in the HDF-EOS format, and are distributed on CD-ROM, DVD, DLT, 8-mm tape, and file transfer protocol (FTP).

The ASTER data have about the same spatial resolution as Landsat, but they provide more spectral bands, which provide scientists with a greater ability to characterize various surface phenomena. Figure 29.8 shows an ASTER image of Washington, DC in color-infrared.

The life expectancy of the EOS Terra mission is 6 years. It will be followed in later years by other EOS spacecraft that take advantage of new developments in remote sensing technologies.

29.4 Image Processing and Geographic Information Systems

Since the early days of monitoring the Earth by orbiting spacecraft, the development of computer-aided techniques for reliably identifying many categories of surface features within a remotely sensed scene, either by photo interpretation of enhanced images or by classification, ranks in itself as an outstanding achievement. Numerous practical uses of such self-contained information are made without strong dependence on other sources of complementary or supporting data. Thus, automated data processing assists in recognizing and mapping, for example, major crop types, estimating their yields, and spotting early warning indicators of potential disease or loss of vigor.

However, many applications, particularly those involving control of dynamic growth or change systems, decision making in management of natural resources, or exploration for nonrenewable energy or mineral deposits, require a wide variety of input data (from multiple sources) not intrinsic to acquisition by space-borne sensors such as those on Landsat, the commercial satellite SPOT, and others of similar purpose. Data from remote sensing satellites combined in a geographic information system with geospatial data on themes such as soils, terrain, geology, and hydrology provide the means for characterizing the land surface over extended areas.

Some data are essentially fixed or time-independent—slope, aspect, rock types, drainage patterns, archaeological sites, etc.—in the normal span of human events. These data are usually collected and shown on maps. When digitized, they are included as layers in a GIS. Other data come from measurements or inventories conducted by people on the ground or in the air—such as weather information, population censuses, soil types and so forth. These too can be incorporated as GIS data layers. However, many vital data are transient or ephemeral—crop growth, flood water extent, insect infestation, limits of snow cover, etc.—and must be collected in a timely sense. Remote sensing data play a key role in this last instance, and in fact satellite monitoring is often the only practical and cost-effective way to acquire frequent data over large regions.

Using these tools we can relate GIS data layers and features shown on remote sensing imagery. For example, Fig. 29.9 (BGS and DPHE 2001) shows a map of arsenic concentrations in shallow water wells in Bangladesh. Comparing this map with the Landsat image of Bangladesh

Fig. 29.8 ASTER image of Washington, DC (Courtesy NASA)

(Fig. 29.10), one can see that the areas of high arsenic concentrations correspond with the coastal flood plains of the country (see also Chap. 12, this volume).

29.5 Landscape Ecology and Disease Systems

Vector-borne diseases usually have complex life cycles (Fig. 29.11). For any given system, the host(s), vector(s), and pathogen are each subjected to a variety of "pressures" within the ecosystem. Many environmental factors drive or constrain the system: weather and climate, food and space resources, predators, and parasites. For example, vertebrate hosts are affected by food quantity and quality, availability of nesting sites, and exposure to predators or parasites. The vector is affected by temperature, humidity, food resources (which may differ between adult and immature stages), and by predators and parasites. The pathogen is affected by host immune status and the frequency and timing of contact between vector and host. Temperature has a major impact on the development rate of the pathogen when it is developing in the vector. With the exception of vector-borne diseases that have humans as the primary or only vertebrate host (e.g., malaria, dengue, and bancroftian filariasis), humans often become involved in the transmission cycle by accident, and do not develop sufficient parasitemia or viremia to infect additional vectors; that is, they are "dead-end" hosts (see also Chap. 20, this volume).

Landscape ecology deals with the mosaic structure of landscapes and ecosystems, and considers the spatial heterogeneity of biotic and abiotic components as the underlying mechanism that determines the structure of ecosystems (Forman and Godron 1986; Kitron 1998). Vector-borne diseases are complex in their spatial and temporal distribution (Fig. 29.12). All components of the system, pathogen, vector, and host must occur together in time and space for epizootics or epidemics to occur. Variations in landscape structure create a patchwork of suitable and unsuitable habitats, which lead to focal disease activity. Barriers, such as water bodies, deserts, or mountain ranges, may prevent the occurrence of a pathogen in an otherwise suitable location. Remotely sensed images of the land, coupled with other geographic data that characterize the landscape, help us to understand the ecosystem structure and to identify areas where risk of disease is greater.

29.6 Relating the Disease Cycle to the Underlying Physical Environment

GIS, global positioning systems (GPS), remote sensing, and spatial statistics provide techniques and methods that we can use to analyze and integrate the spatial component into studies of the ecology and epidemiology of vector-borne disease (Kitron 1998). These spatial tools, together with the concepts of landscape ecology, can help us to better

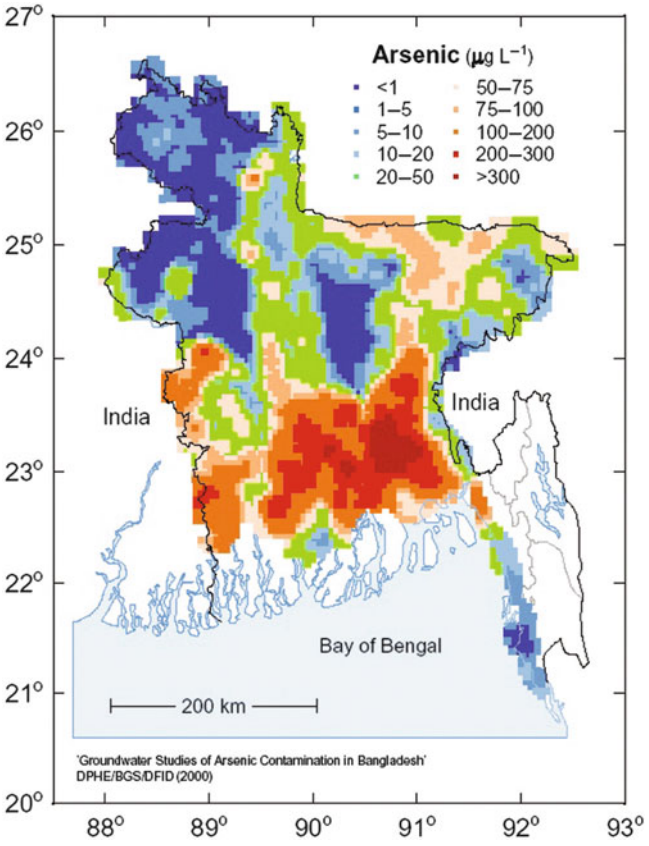

Fig. 29.9 Arsenic concentrations in groundwater in Bangladesh (Courtesy BGS)

understand emerging infectious diseases as well as the potential impact of global change on vector-borne diseases.

Several studies have utilized satellite-derived estimates of ground temperature and moisture to predict the distribution or risk of vector-borne disease. Malone et al. (1997) used an annual time series of diurnal temperature difference (dT, derived from day-night pairs of AVHRR data) to map high and low prevalence zones of the parasite, *Schistosoma mansoni* in Egypt. The dT values were associated with the depth of the water table, a major environmental determinant of the distribution of this water and snail-associated parasite.

Lindsay and Thomas (2000) characterized the climate at sites in Africa where surveys for lymphatic filariasis had taken place by using computerized climate surfaces. Logistic regression analysis of the climate variables predicted with 76% accuracy whether sites had microfilaremic patients or not. A map of the risk of lymphatic filariasis infection across Africa, built from the logistic equation in a GIS, compared favorably with expert opinion. A further validation, using a quasi-independent data set, showed that the model correctly predicted 88% of the infected sites. They then used a similar procedure to map the risk of microfilaremia in Egypt, where the dominant vector species differs from those in sub-Saharan Africa. By overlaying risk maps on a 1990 population grid, and adjusting for recent population increases, they estimated that around 420 million people would be exposed to this infection in Africa in the year 2000. The approach described by these authors could be used to produce a sampling frame for conducting filariasis surveys in countries that lack accurate distribution maps.

Fig. 29.10 Landsat image of Bangladesh (Courtesy USGS)

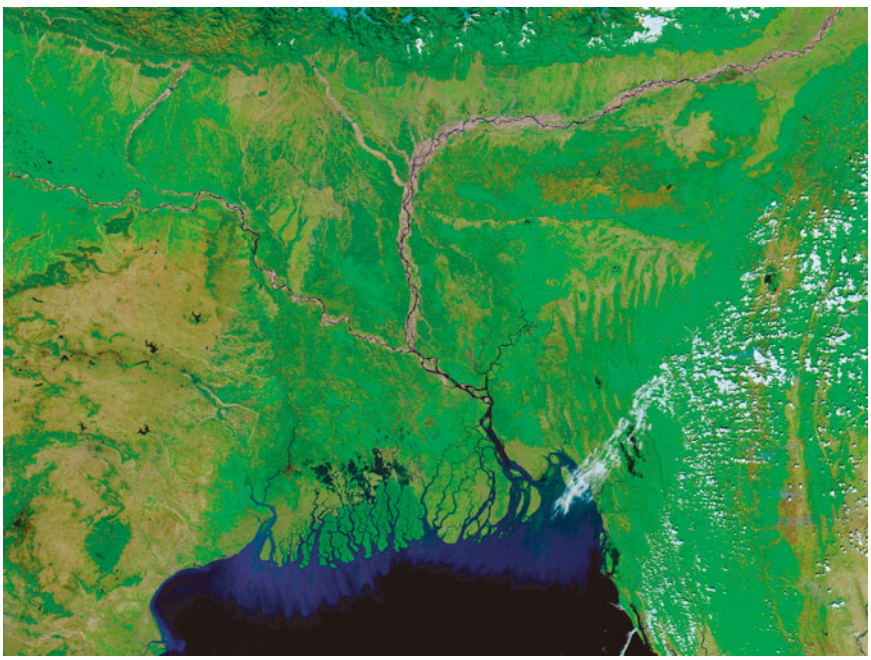

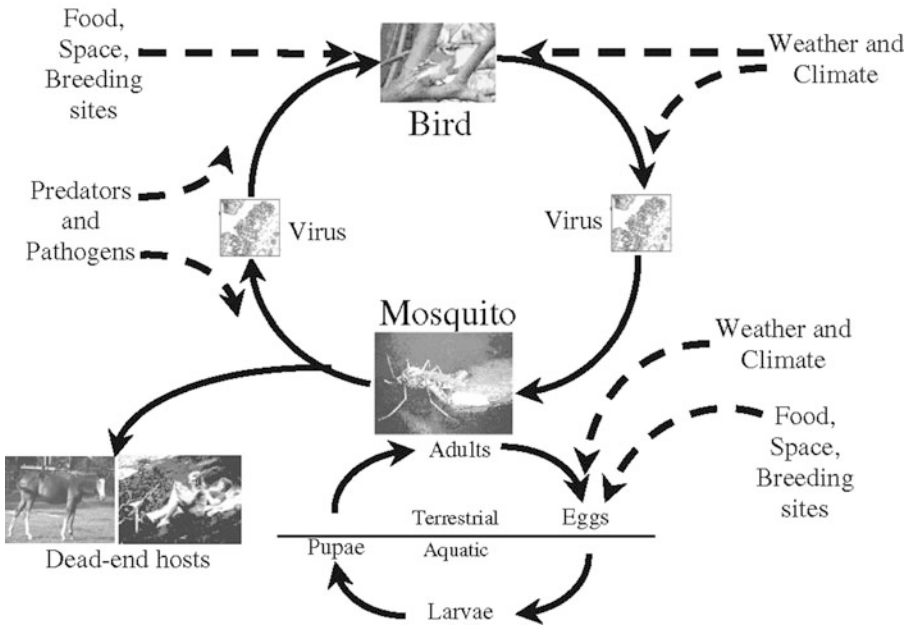

Fig. 29.11 A typical arbovirus cycle showing sources of environmental pressure on the system

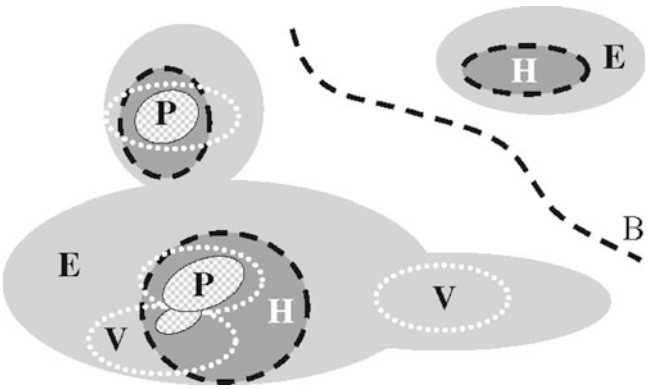

Fig. 29.12 Spatial relationships in the arbovirus-vector-host ecosystem. All components are limited by a suitable environment (*E*). Populations of the vertebrate host (*H*) do not necessarily overlap with the distribution of the vector (*V*). It is only in those regions of *E* where both *H* and *V* overlap that the pathogen (*P*) can survive. Barriers (*B*) to dispersal may limit the presence of *V* or *H*

American and Mexican researchers collaborated in a study to map habitats of the malaria vector, *Anopheles albimanus*, using Landsat Thematic Mapper (TM) imagery and extensive ecological and epidemiological data (Beck et al. 1994). Pixel categories were associated with landscape type both by ground surveys and by comparison to color-infrared photography of the study area. Since the relationship between landscape type and suitability as larval habitat for *Anopheles albimanus* was very strong, it was possible to correctly distinguish between villages with high and low vector abundance with an overall accuracy of 90%. These analyses indicated that the most important landscape elements in terms of explaining mosquito abundance were the proportions of transitional wetlands and unmanaged pasture. Using these two landscape elements as predictors, they were able to correctly distinguish villages with high and low mosquito abundance with an overall accuracy of 90%.

Robinson et al. (1997) mapped the distribution of tsetse (*Glossina* spp.) habitat by using climate and remotely sensed vegetation data. Coarse-resolution (7.6 km) AVHRR images were combined with smoothed climate surfaces derived from continent-wide, long-term weather station records. Predictions were improved by subdividing habitats prior to classification. This system might be improved by using satellite-derived weather data and by using finer grain imagery (e.g., 1.1 km AVHRR).

Several groups have used remotely sensed data to improve our understanding of Lyme disease. Glass et al. (1992), for example, conducted a case–control study of Lyme disease in Baltimore County, Maryland. Land use/land cover maps (derived from Landsat TM imagery) were combined with soils, elevation, geology, and watershed maps to evaluate risk of exposure to Lyme disease and its vector, *I. scapularis*. The risk of disease was significantly lower in highly developed areas, and risk decreased with increasing distance from forests. Dister et al. (1997) used Landsat TM images to evaluate Lyme disease exposure risk on 337 residential premises in two communities in Westchester County, New York. Premises were categorized as no, low, or high risk based on seasonally adjusted densities of *I. scapularis* nymphs (previously determined by sampling). Spectral indices from the TM scene provided relative measures of vegetation structure and moisture (wetness) as

well as vegetation abundance (greenness). They used GIS to spatially quantify and relate the landscape variables to risk category. A comparison of the two communities showed that the community with more high-risk premises was significantly greener and wetter than the community with fewer high-risk premises. Furthermore, high-risk premises were significantly greener and wetter than lower risk premises in the high-risk community. The high-risk sites appeared to contain a greater proportion of broadleaf trees, while lower risk sites were interpreted as having more non-vegetative cover or open lawn. The ability to distinguish these fine-scale differences among communities and individual properties illustrates the efficiency of a remote sensing/GIS-based approach for identifying peridomestic risk of Lyme disease over large geographic areas.

More recently, Moncayo et al. (2000) combined Landsat TM images with aerial videography to generate a map of landscape elements around 15 human and horse cases of eastern equine encephalomyelitis (EEE) in southeastern Massachusetts. EEE exists in enzootic foci transmitted between birds and the mosquito, *Culiseta melanura* (the enzootic vector). In Massachusetts and surrounding states, epidemic/epizootic transmission may involve as many as six additional mosquito species (*Aedes canadensis*, *Aedes vexans*, *Culex salinarius*, *Coquillettidia perturbans*, *Anopheles quadrimaculatus*, and *Anopheles punctipennis*), each with its characteristic larval and adult habitat requirements. Stepwise regression analysis showed that wetlands and more specifically, deciduous wetlands, were the most important major class element. Deciduous wetlands accounted for up to 72.5% of the observed variation in the host-seeking populations of *A. canadensis*, *A. vexans*, and *C. melanura*. The authors propose combining habitat mapping with street maps to identify and prioritize areas in need of vector mosquito control.

Even coarse-grain satellite imagery can be used to advantage. Daniel and Kolár (1990) analyzed a 25-year database on the distribution and abundance of *I. ricinus*, the vector of tick-borne encephalitis in Europe, in relation to land cover types derived from a 41 × 41 km section of a Landsat multispectral scanner (MSS) scene. They showed that *I. ricinus* is associated with specific land cover types, which allowed them to generate risk maps that could be used in public education and other prevention programs.

29.7 Technical Issues and Limitations

29.7.1 Analytical and Statistical Issues

Although a picture may be worth a thousand words, it is still necessary to know whether the patterns we think we see are, in fact, statistically significant rather than the result of random noise. Better integration of GIS and spatial statistics software would be advantageous, but it is probably not desirable or economically feasible for each GIS package to integrate a spatial statistics module. Rather, it would be helpful for developers from the two fields to agree upon common import/export formats to permit the rapid movement of data between the two types of software. Bailey (1994) provides a good review of progress in the integration of spatial statistics and GIS. As the focus of GIS and remote sensing in vector-borne disease moves from description to prediction, there will be a greater need for analytical techniques that simultaneously deal with space and time. Cressie (1996) identified several issues and approaches to dealing with spatiotemporal processes.

29.7.2 Modeling and Simulation

Perhaps the greatest potential for applying remotely sensed information to the surveillance, prediction, and control of vector-borne and zoonotic diseases is the ability to use these data in predictive models. Models come in a great variety, and it is crucial to use the right type of model to answer a specific question. Thus, models designed to elucidate the mechanism of a particular ecological process may not be good predictive models and vice versa. An area where considerable progress is being made is in landscape ecology, where issues of sustainable harvestable resources and preservation of endangered species habitats have become crucial. A good survey of theory and applications in this area can be found in Turner and Gardner (1991).

29.7.3 Temporal and Spatial Resolution

The spatial scale of satellite imagery should match the scale of the object of study at ground level. Early remote sensing studies (e.g., Hayes et al. 1985) were limited to Landsat MSS images, with a pixel resolution of about 80 m. This placed severe limitations on the size of habitats that could be detected. Today, with the advent of commercial imagery with 1-m resolution, the lack of sufficient high-resolution, ground-level data has become a limiting factor in the application of remote sensing to solving issues in vector-borne disease ecology.

29.7.4 The Issue of Scale

Ecological phenomena exhibit patterns at different scales (e.g., Turner et al. 1991; Quattrochi and Goodchild 1997). Vector-borne diseases are no exception to this phenomenon (Korenberg 1989). Thus, a virus-vector-vertebrate host

system, such as LaCrosse encephalitis, can exhibit distributional pattern at the continental scale, the regional scale, and at the local scale (Fig. 29.13). For a given question or hypothesis about any disease, there is probably an optimal scale at which to measure the system components. Thus, it is crucial to clearly understand the scale(s) at which different components of the disease system operate.

29.7.5 Imagery Issues

The resolution of remotely sensed imagery may not be satisfactory for studies at a particular scale. Resolution here can refer to space, time, or spectral composition. In particular, studies of some diseases, such as dengue and LaCrosse encephalitis, would benefit from the ability to identify water-holding containers on individual premises. This can be accomplished by using high-resolution aerial photography, but temporal coverage will be sparse due to the high cost of flying such missions. Also, the spectral coverage will be very narrow, which reduces the utility of the imagery.

Cloud cover and other disturbances are a perennial problem. One anticipated use of remote sensing is in evaluating the threat of disease outbreaks following floods, hurricanes, or other natural disasters. Because many of these disasters are weather related, it is not uncommon for the areas of interest to be completely covered by clouds for weeks following the event. Perhaps additional studies on the use of real-time radar in conjunction with historical imagery in other spectral regions or similar systems could improve prospects for using remote sensing in this setting (e.g., Imhoff and McCandless 1988).

Landscape feature classification is an important tool for understanding and modeling vector-borne and zoonotic diseases. One or more specific land cover types (e.g., scrub, piñon-juniper, oak-hickory forest, etc.) often define these diseases. Thus, it is important to be able to distinguish between cover types. All of the problems related to slope, aspect, and shading as they impact the remotely sensed image also need to be dealt with. Soil type, elevation, slope, and aspect often have a major impact on the distribution of vertebrate hosts of these disease agents, especially small mammals. It should be possible, at least in theory, to infer some of these qualities from the remotely sensed spectral signals, particularly from hyperspectral imagery.

29.7.6 Ground Data Issues

One of the first things that strikes the entomologist or epidemiologist when looking at remotely sensed imagery is the enormous amount of information in comparison to the available data on the diseases we would like to study. For many diseases, such as cancer and birth defects, there are well-developed registries that give detailed information about cases. Such information allows the epidemiologist to search for associations between environmental indicators (from the remotely sensed data) and the location of cases. Unfortunately, reporting systems for vector-borne diseases are generally poorly developed or entirely absent. For example, dengue which, as reported above, is responsible for as many as 50–100 million cases each year, is not even reported in many countries. Only the more severe cases are entered into the reporting system. Even in the United States, the vector-borne diseases are generally grossly underreported. To successfully apply remote sensing to the surveillance, prevention, and control of vector-borne and zoonotic diseases, we need well-designed surveillance systems to provide the "ground truth" data to validate the models that are being developed.

29.7.7 Privacy Issues

A separate but extremely important issue relating to the collection of disease surveillance data is the issue of privacy. There is concern on the part of some citizens that their personal privacy would be violated by having the precise location of their residence, school, workplace, etc., entered into a database, particularly if that information in also associated with health-related information. Thus, many reporting systems show only the city or county of residence. This severely limits the utility of the data for remote sensing studies.

One way to bypass this problem, at least with the vector-borne and zoonotic diseases, is to monitor disease activity in the vector or the wild vertebrate host (in some situations, susceptible domestic animals can also be monitored). Detailed protocols have been developed for collecting the appropriate data from these parts of the disease system (e.g., Moore et al. 1993; Moore and Gage 1996). Data from these field-oriented surveillance systems can be used to predict disease activity in the human (or domestic animal) population. Because these surveillance systems are generally removed in space (often rural) and time (activity precedes disease in humans) from the human population at risk, there is often a shortage of funding and staffing for these programs. Thus, the surveillance agency wants to collect as much useful information as possible in the shortest number of hours with the smallest possible work force. To do this, programs are increasingly moving to automated field data recording systems, GPS, and similar equipment to reduce paperwork, data entry error, and similar time-consuming problems. The Centers for Disease Control is currently funding the development of an integrated database, GIS,

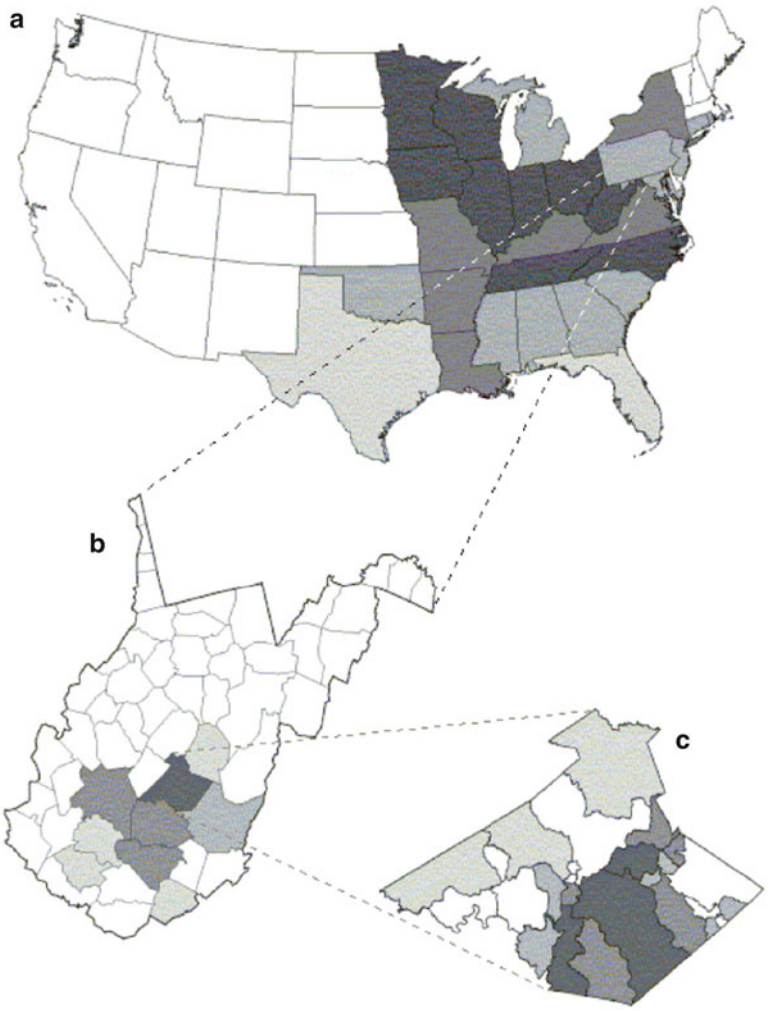

Fig. 29.13 Effect of scale on pattern and distribution of LaCrosse encephalitis in the United States; patterns are evident at several spatial levels. *Darker colors* indicate more viral activity

and decision support system that will speed the collection of vector-borne disease related data. Once completed, the system, called the National Electronic Arbovirus Reporting System (NEARS), will be accessible via the Worldwide Web. Data at differing spatial resolutions can be downloaded for use with remotely sensed data.

29.8 Prospects for the Future

The utility of remotely sensed data for improving our understanding, prevention, and control of vector-borne and zoonotic diseases has been abundantly demonstrated. Even greater opportunities exist for applying the imagery from current and future remote-sensing platforms. Much of the eventual progress in applying that imagery to the solution of human problems, including the diseases of interest to us, will depend on the priorities set by universities, governments, and funding agencies. There is a need for cross-disciplinary programs in universities to provide qualified and broadly trained researchers for this growing field. Collaborative research, within and between agencies and departments, should be encouraged. It is no longer possible for a single researcher or a small group within a single discipline to "do it all." By sharing valuable resources and insights (expertise), progress can be more rapid and costs can be reduced.

See Also the Following Chapters. Chapter 12 (Arsenic in Groundwater and the Environment) • Chapter 20 (The Ecology of Soil-Borne Human Pathogens) • Chapter 28 (GIS in Human Health Studies)

References and Further Reading

Bailey TC (1994) A review of statistical spatial analysis in geographical information systems. In: Fotheringham S, Rogerson P (eds) Spatial analysis and GIS. Taylor and Francis, London, pp 13–44

Beck LR, Rodriguez MH, Dister SW, Rodriguez AD, Rejmankova E, Ulloa A, Meza RA, Roberts DR, Paris JF, Spanner MA, Washino RK, Hacker C, Legters LJ (1994) Remote sensing as a landscape epidemiologic tool to identify villages at high risk for malaria transmission. Am J Trop Med Hyg 51:271–280

Beck LR, Lobitz BM, Wood BL (2000) Remote sensing and human health: new sensors and new opportunities. Emerg Infect Dis 6 (3):217–227

BGS, DPHE (2001) Arsenic contamination of groundwater in Bangladesh. In: Kinniburgh DG, Smedley PL (eds) British Geological Survey technical report WC/00/19. British Geological Survey, Keyworth

Clarke KC, McLafferty SL, Tempalski BJ (1996) On epidemiology and geographic information systems: a review and discussion of future directions. Emerg Infect Dis 2:85–92

Cline BL (1970) New eyes for epidemiologists: aerial photography and other remote sensing techniques. Am J Epidemiol 92:85–89

Colwell RR (1996) Global climate and infectious disease: the cholera paradigm. Science 274:2025–2031

Cressie N (1996) Statistical modeling of environmental data in space and time. In: Mowrer HT, Czaplewski RL, Hamre RH (eds) Spatial accuracy assessment in natural resources and environmental sciences: second international symposium, U.S. Department of Agriculture, Forest Service, GTR RM-GTR-277, Fort Collins, CO, pp 1–3

Daniel M, Kolár J (1990) Using satellite data to forecast the occurrence of the common tick *Ixodes ricinus* (L.). J Hyg Epidemiol Microbiol Immunol 34:243–252

Dister SW, Fish D, Bros SM, Frank DH, Wood BL (1997) Landscape characterization of peridomestic risk for Lyme disease using satellite imagery. Am J Trop Med Hyg 57(6):687–692

Estes JE, Loveland TR (1999) Characteristics, sources, and management of remotely-sensed data. In: Longely PA, Goodchild MF, Maguire DJ, Rhind DW (eds) Geographical information systems, 2nd edn. Wiley, New York, pp 667–675

Forman RTT, Godron M (1986) Landscape ecology. Wiley, New York

Glass GE, Morgan JM III, Johnson DT, Noy PM, Israel E, Schwartz BS (1992) Infectious disease epidemiology and GIS: a case study of Lyme disease. GeoInfoSystems 2:65–69

Gratz NG (1999) Emerging and resurging vector-borne diseases. Annu Rev Entomol 44:51–75

Hayes RO, Maxwell EL, Mitchell CJ, Woodzick TL (1985) Detection, identification and classification of mosquito larval habitats using remote sensing scanners in earth-orbiting satellites. Bull WHO 63:361–374

Imhoff ML, McCandless SW (1988) Flood boundary delineation through clouds and vegetation using L-band space-borne radar: a potential new tool for disease vector control programs. Acta Astronaut 17:1003–1007

Jetten TH, Focks DA (1997) Potential changes in the distribution of dengue transmission under climate warming. Am J Trop Med Hyg 57:285–297

King M (2000) EOS measurements, National Aeronautics and Space Administration, Goddard Space Flight Center. http://eospso.gsfc.nasa.gov/ftp_docs/measurements.pdf

Kitron U (1998) Landscape ecology and epidemiology of vector-borne diseases: tools for spatial analysis. J Med Entomol 35(4):435–445

Korenberg EI (1989) Population principles in research into natural focality of zoonoses. Sov Sci Rev F Physiol Gen Biol 3:301–351

Lindsay SW, Thomas CJ (2000) Mapping and estimating the population at risk from lymphatic filariasis in Africa. Trans R Soc Trop Med Hyg 94(1):37–45

Linthicum KJ, Anyamba A, Tucker CJ, Kelley PW, Myers MF, Peters CJ (1999) Climate and satellite indicators to forecast Rift Valley fever epidemics in Kenya. Science 285:397–400

Malone JB, Abdel-Rahman MS, El Bahy MM, Huh OK, Shafik M, Bavia M (1997) Geographic information systems and the distribution of *Schistosoma mansoni* in the Nile delta. Parasitol Today 13:112–119

Martens WJM, Niessen LW, Rotmans J, Jetten TH, McMichael AJ (1995) Potential risk of global climate change on malaria risk. Environ Health Perspect 103:458–464

Moncayo AC, Edman JD, Finn JT (2000) Application of geographic information technology in determining risk of eastern equine encephalomyelitis virus transmission. J Am Mosq Control Assoc 16(1):28–35

Moore CG, Gage KL (1996) Collecting methods for vector surveillance. In: Beaty BJ, Marquardt WC (eds) The biology of disease vectors. University Press of Colorado, Niwot, pp 471–491

Moore CG, McLean RG, Mitchell CJ, Nasci RS, Tsai TF, Calisher CH, Marfin AA, Moore PS, Gubler DJ (1993) Guidelines for arbovirus surveillance in the United States. U. S. Dept. of Health and Human Services/Centers for Disease Control, Fort Collins

Ostfeld RS, Jones CG, Wolff JO (1996) Of mice and mast: ecological connections in eastern deciduous forests. Bioscience 46:323–330

Pope KO, Rejmankova E, Savage HM, Arredondo-Jimenez JI, Rodriguez MJ, Roberts DR (1994) Remote sensing of tropical wetlands for malaria control in Chiapas, Mexico. Ecol Appl 4:81–90

Quattrochi DA, Goodchild MF (eds) (1997) Scale in remote sensing and GIS. Lewis Publishers, Boca Raton

Reeves WC, Hardy JL, Reisen WK, Milby MM (1994) Potential effect of global warming on mosquito-borne arboviruses. J Med Entomol 31:324–332

Robinson T, Rogers D, Williams B (1997) Mapping tsetse habitat suitability in the common fly belt of Southern Africa using multivariate analysis of climate and remotely sensed vegetation data. Med Vet Entomol 11:235–245

Shope RE (1992) Impacts of global climate change on human health: spread of infectious diseases. In: Majumdar SK, Kalkstein LS, Yarnal B, Miller EW, Rosenfeld LM (eds) Global climate change: implications, challenges and mitigation measures. Pennsylvania Academy of Science, Easton, pp 361–370

Short NM (ed) (2003) The remote sensing tutorial. National Aeronautics and Space Administration/Goddard Space Flight Center, Greenbelt

Srivastava A, Nagpal BN, Saxena R, Sharma VP (1999) Geographic information system as a tool to study malaria receptivity in Nadiad Taluka, Kheda District, Gujarat, India. Southeast Asian J Trop Med Public Health 30(4):650–656

Star JL, Estes JE, Davis F (1991) Improved integration of remote sensing and geographic information systems: a background to NCGIA initiative 12. Photogramm Eng Remote Sens 57:643–645

Turner MG, Gardner RH (eds) (1991) Quantitative methods in landscape ecology. Springer, New York

Turner SJ, O'Neill RV, Conley W, Conley MR, Humphries HC (1991) Pattern and scale: statistics for landscape ecology. In: Turner MG, Gardner RH (eds) Quantitative methods in landscape ecology. Springer, New York, pp 17–49